

Cyclic behavior and performance of a coupled-steel plate shear wall with fuse pin

Mahdi Usefvand ^{1a}, Ahmad Maleki ^{*1} and Babak Alinejad ^{2a}

¹ Department of Civil Engineering, Maragheh Branch, Islamic Azad University, Maragheh, Iran

² Department of Civil Engineering, University of Maragheh, Maragheh, Iran

(Received July 22, 2020, Revised July 10, 2021, Accepted August 2, 2021)

Abstract. Coupled steel plate shear wall (C-SPSW) is one of the resisting systems with high ductility and energy absorption. Energy dissipation in the C-SPSW system is accomplished by the bending and shear behavior of the link beams and SPSW. Energy dissipation and floor displacement control occur through link beams at low seismic levels, easily replaced after an earthquake. In this study, a coupled steel plate shear wall with a yielding fuse is presented. The system uses a high-ductility fuse pin element instead of a link beam, which has good replaceability after the earthquake. In this study, four models of coupled steel plate shear walls were investigated with I-shaped link beam, I-shaped link beam with reduced beam section (RBS), box-link beam with RBS, and fuse pin element under cyclic loading. The finite element method was used through ABAQUS software to develop the C-SPSW models. To verify the finite element model results, two test specimens of coupled steel plate shear walls were validated. Comparative results of the hysteresis curves obtained from the finite element analysis with the experimental curves indicated that the finite element model offered a good prediction of the hysteresis behavior of C-SPSW. The results of the C-SPSW models revealed that the fuse pin caused an increase in the ultimate capacity by approximately 19% and the energy dissipation by 20% compared to the other C-SPSW.

Keywords: Coupled steel plate shear wall (C-SPSW); energy dissipation; fuse; finite element method

1. Introduction

Steel plate shear walls (SPSWs) with high ductility and high energy dissipation are used as a lateral-resistant structural system (Gorji Azandariani *et al.* 2021e). In SPSWs, they can characterize their high ductility, strength, initial hardness, stable behavior in cyclic loading, and energy absorption. Fig. 1 illustrates the types of common steel shear wall systems. Common SPSW systems include SPSW with simple connections beam-column, SPSW with a rigid beam-column connection, and SPSW with a coupling system. In the meantime, new types of reduced beam section moment connections after the Northridge and Kobe earthquakes SPSW and steel moment frame systems have also become customary (Hassanipour *et al.* 2015, Rahnavard *et al.* 2015). Many researchers have investigated the performance of the SPSW and the effect of various parameters affecting its behavior using numerical and experimental methods (Dhar and Bhowmick 2016, Elgaaly *et al.* 1993, Gorji Azandariani *et al.* 2020b, 2021a, b, c, e, Lubell *et al.* 2000, Park *et*

*Corresponding author, Ph.D., E-mail: Ah_Maleki@yahoo.com

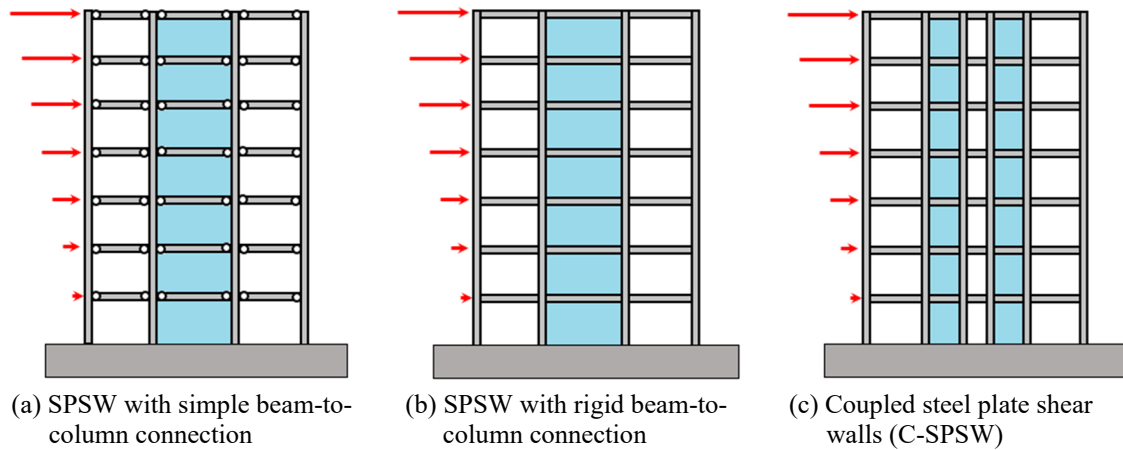


Fig. 1 Types of steel shear walls (SPSWs) system

al. 2007, Qin *et al.* 2017, Shekastehband *et al.* 2017, Talebizadehsardari *et al.* 2020, Vatansever and Berman 2015, Vatansever and Yardimci 2011). The coupled steel plate shear wall (C-SPSW) system consists of two separate shear walls connected by link beams (Fig. 1(c)). The C-SPSW system has high ductility with a very good performance. In the C-SPSW system, the lateral force is distributed across the floors based on the stiffness and strength of the steel infill wall, bending frame, and link beams. The resistance to lateral forces at the C-SPSW occurs through a combination of the flexural behavior of the steel frame and the shear behavior of the steel infill wall and link beams (Borello and Fahnestock 2012, 2013, Li *et al.* 2011, 2012).

Rahnavard *et al.* (2016) conducted nonlinear numerical studies on composite steel-concrete shear walls affecting cyclic loading. Five types of three-dimensional finite element models are developed using ABAQUS emphasizing constitutive material modeling and element type to represent the real physical behavior of complex shear wall structures. This study is investigated important parameters such as concrete failure, hysteresis response, out-of-plane displacement, frame drift, and dissipated energy. The results of the study of Rahnavard *et al.* (2016) showed that steel frames with concrete on one side of the shear plate had better dissipation energy function than other types. The link beam is used as a fuse for energy absorption, and dissipation caused by the earthquake in eccentrically braced frames used. Rahnavard *et al.* (2017) presented single and double shear panels as the seismic fuses for use in eccentrically braced frames. Most of the numerical and experimental work done on the link beams has been performed through cyclic tests to estimate its rotational capacity (Hjelmstad and Popov 1983, Ji *et al.* 2016, 2017, Malley and Popov 1984, Mohebkhah and Azandariani 2020, Okazaki *et al.* 2005, Popov and Engelhardt 1988). Details and design code for link beam are provided in the AISC 314 (2016) based on the type of link beam behavior. According to the AISC 314 (2016), link beam behavior is subdivided into three zones: shear, flexural-shear, and flexural. Dubina and Dinu (2014), Dimakogianni *et al.* (2015), and Dougka *et al.* (2014) presented a new energy dissipation system to improve the seismic behavior of the moment frames. In the proposed system, the fuse pin element was used for the link beams. The fuse pin element was designed to be easily replaceable and repairable with hysteretic behavior and suitable energy dissipation (Dimakogianni *et al.* 2015, Dougka *et al.* 2014). An innovative C-SPSW with a fuse pin element system has been presented to improve the performance of C-SPSWs behavior. The innovative system of coupled steel plate shear wall (C

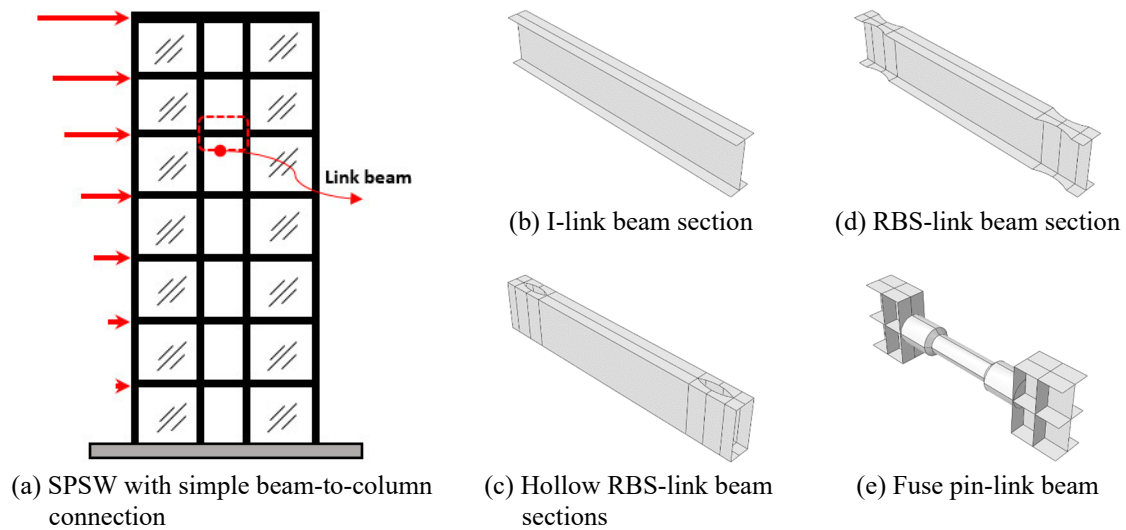


Fig. 2 Types of link beams in C-SPSWs

SPSW) with fuse pin in the link beam (CF-SPSW) consists of C-SPSW in which the link beam of fuse pin element presented by Dougka *et al.* (2014) is used (Fig. 2). The proposed system CF-SPSW as a lateral load-resistant system at the low seismic level by yielding fuse pin element provides protection against SPSW damage. Thus, at low seismic levels, the system allows the steel shear wall stiffness to limit the relative displacements of the floors where the yielding fuse of link beams for energy dissipation is used. The use of the fuse pin element in the C-SPSW as an alternative fuse and easy repair with hysteretic behavior and high energy absorption can be noted.

In this study, the cyclic behavior of the coupled steel plate shear walls with a fuse pin in the link beam (C-SPSW) is investigated. For this purpose, a 12-story C-SPSW structure is designed according to AISC 314 (2016), and the last three floors are selected for the cyclic behavior analysis. The finite element method and ABAQUS (2010) software have been used to study the cyclic behavior of the models C-SPSW. Validation for the results of finite element models has been performed with test results. For validation of numerical models, Dubina and Dinu (2014) experimental specimens were used. Finite element models include coupled steel plate shear walls with I-shaped link beam, I-shaped link beam with reduced beam section (RBS), hollow-link beam with RBS, and fuse pin-link beam (Fig. 2). The results of finite element models include hysteresis diagrams, lateral stiffness, and damped energy. Finally, the results of finite element models present hysteresis curves, lateral stiffness, and energy dissipation.

2. Design of the C-SPSW structure

In this section, to investigate the cyclic behavior of the C-SPSW following Fig. 3, three layers of full-scale 12-story C-SPSW structures are selected. To this end, in this section, details of the design of the C-SPSW structure are presented. The structural coupled C-SPSWs, the plan, and the prototype with details of span and height dimensions are shown in Fig. 3. As shown in Fig. 3, for the frames adjacent to the C-SPSW, a simple weight-bearing frame system is used; thus, only the C-SPSW is considered a lateral load-resistant system. The perimeter gravity frame bays, 5.0 m

long, the SPSW bay, 5.0 m long, and the link beam bay, 2.5 m long, are considered from the center to center of the columns. The 12 stories of the building are considered to have uniform heights of 4.0 m. C-SPSW was designed according to the recommendations given in AISC Seismic Provisions (2016) and AISC Design Guide 20 (2007).

The Canadian Standards Association (CAN/CSA S16-01/2001) (2009) and the AISC Seismic Provisions (2016) have adopted the SPSW as a lateral-resistant structural system. In the Canadian Standards Association (CAN/CSA S16-01/2001) (2009) and the AISC Seismic Provisions (2016), for the design of SPSWs, the initial design of beam sections, columns, and infill plates are performed similar to a tensile brace. Hence, instead of each steel infill plate, an equivalent tensile brace is considered. After determining the cross-sectional area of each tensile brace, the AISC Design Guide 20 (2007) recommends Eq. (1) to calculate the thickness of the steel infill plate as follows

$$t = \frac{2A_b \sin\theta \sin 2\theta}{L \sin^2 2\alpha} \quad (1)$$

where θ is the angle between the brace and the column, L shows the width of the frame opening, A_b represents the cross-sectional area of the brace is equivalent, and α denotes the angle of formation of the diagonal tensile field in the steel infill plate obtained from Eq. (2) as follows

$$\tan^4 \alpha = \frac{1 + \frac{t_w L}{2A_c}}{1 + t_w h \left(\frac{1}{A_b} + \frac{h^3}{360 I_c L} \right)} \quad (2)$$

where A_c and I_c reflect the cross-section and moment of inertia of the side columns, h is the height of the floor, and A_b represents the cross-section of the beam. After determining the thickness of the plate, according to the AISC Design Guide, 20 (2007) is used for analysis and design. The cross-sectional area of each strip is obtained from Eq. (3)

$$A_s = \frac{L \cos \alpha + h \sin \alpha}{n} \cdot t \quad (3)$$

where n the number of strips is equal to 10 diagonal strips for C-SPSW analysis. It also proposes AISC Design Guide 20 (2007) and Eq. (4) to the stiffness of the columns for preventing column buckling under the influence of the diagonal tensile field.

$$I_c \geq \frac{0.00307 t h^4}{L} \quad (4)$$

The use of residential structures is assumed, and the gravity loading of the model and the floor loader system is assumed to be composite slabs weighing 500 kg/m^2 . The live load of the floors is 200 kg/cm^2 and the live roof load was considered 150 kg/cm^2 . The seismic base shear, V_E , was calculated according to the Iranian seismic building code (Standard 2800) (2014), which is similar to the code ASCE7-10 (2010). Load combinations were based on Regulations ASCE7-10 (2010) where a combination of 1.2D+1.6L, 1.2D+1.0L+1.0E, and 0.9D+1.0E was considered. American W-sections were used for beam and column design sections. The sections designed for the coupled steel plate shear wall are presented in Table 1. The assumed materials for modeling and analysis

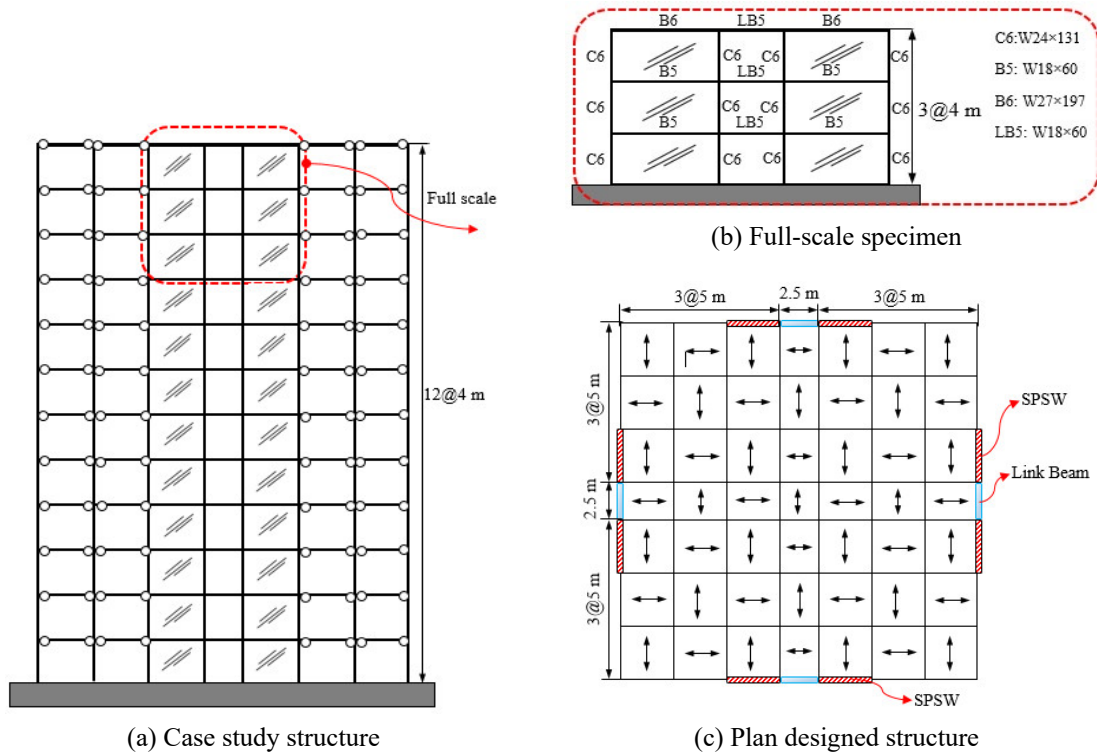


Fig. 3 The C-SPSW structures

Table 1 Designed sections for the C-SPSW

Story	Plate thickness (mm)	Internal column section	External column section	Beam section	Link beam section
1	8	C1: W 33 × 263	C1: W 33 × 263	B1: W 18 × 234	LB1: W 18 × 192
2	8	C1: W 33 × 263	C1: W 33 × 263	B1: W 18 × 234	LB1: W 18 × 192
3	7	C2: W 30 × 261	C2: W 30 × 261	B2: W 18 × 158	LB2: W 18 × 130
4	7	C2: W 30 × 261	C2: W 30 × 261	B2: W 18 × 158	LB2: W 18 × 130
5	6	C3: W 27 × 281	C3: W 27 × 281	B3: W 18 × 106	LB3: W 18 × 97
6	6	C3: W 27 × 281	C3: W 27 × 281	B3: W 18 × 106	LB3: W 18 × 97
7	5	C4: W 24 × 250	C4: W 24 × 250	B4: W 18 × 71	LB4: W 18 × 65
8	4	C5: W 24 × 229	C5: W 24 × 229	B4: W 18 × 71	LB4: W 18 × 65
9	4	C5: W 24 × 229	C5: W 24 × 229	B5: W 18 × 60	LB4: W 18 × 65
10	3	C6: W 24 × 131	C6: W 24 × 131	B5: W 18 × 60	LB5: W 18 × 60
11	3	C6: W 24 × 131	C6: W 24 × 131	B5: W 18 × 60	LB5: W 18 × 60
12	3	C6: W 24 × 131	C6: W 24 × 131	B6: W 27 × 194	LB5: W 18 × 60

were considered for beams and columns sections of S355 steel with 410 MPa yield stress and infill plate of S235 steel with 310 MPa yield stress (Dubina and Dinu 2014).

3. Nonlinear finite element method

An efficient and accurate finite element method should be used to study the cyclic behavior of the C-SPSW system. In this section, a finite element model has been developed using the ABAQUS (2010) software to predict the cyclic behavior of the coupled steel plate shear wall. The modeling sections described below include material properties, loading, boundary conditions, mesh, element type, and the type of analysis.

3.1 Meshing and geometry

ABAQUS (2010) finite element software was used to model the coupled steel plate shear wall experimental specimens and validation. 4-node shell element (S4R) was used for modeling beam, column, and infill plate sections. Mesh sensitivity analysis studies have been performed by Formisano *et al.* (2007) to determine the optimal discretization able to provide the best compromise between the accuracy of the results and the time-consuming analysis. The sensitivity analysis of Formisano *et al.* (2007) shows that the most optimal mesh adopted is the mesh characterized by 25 mm base elements. Therefore, the meshing of the models was considered in 25 mm dimensions for FE models. Each node of this element had six degrees of freedom: three degrees of translational freedom and three degrees of rotational freedom. It also had a 4-node shell element capable of simulating general and local buckling on shear wall infill plates (Ali *et al.* 2018). Fig. 4(a) illustrates the geometry and meshing of the finite element models of experimental specimens in the studies by Dubina and Dinu (2014). In C-SPSW modeling, nonlinear geometry behavior, strain hardening effects, large deformation, and post-buckling behavior were considered for S4R elements. A nonlinear dynamic method (Explicit dynamic) was used to analyze finite element models (Wang *et al.* 2015). This method treats the static problem as a dynamic process and uses the central difference method for gradual integration of structural motion equations,

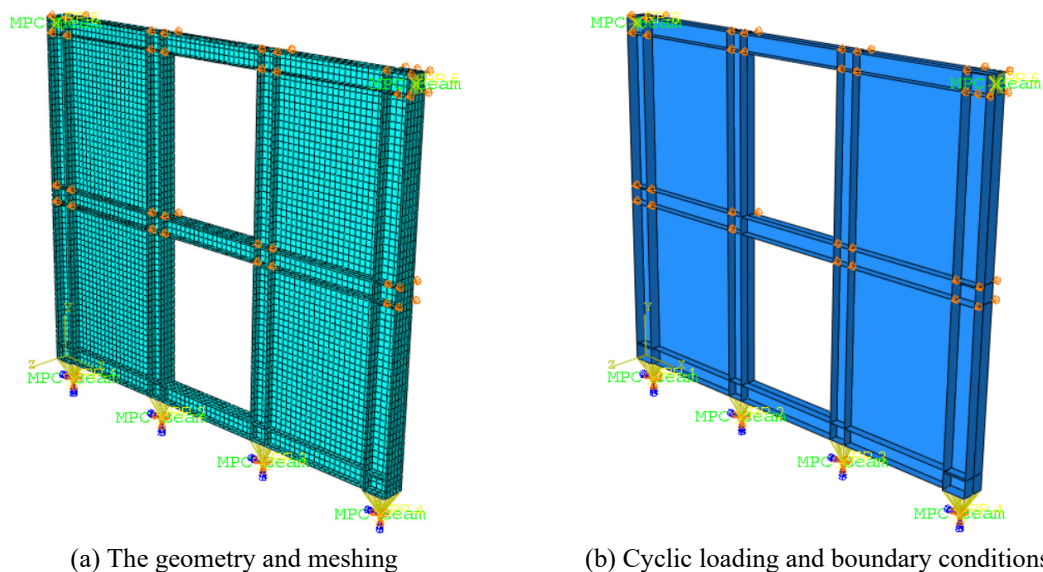


Fig. 4 Finite element models

which is appropriate for solving highly nonlinear problems. The structure density is needed, and an appropriate loading speed is selected as 0.5 every step. The time step size is calculated automatically in ABAQUS, according to the minimum mesh size of models.

3.2 Loading and support conditions

The boundary conditions, including the supports and the cyclic loading applied to the finite element models of the C-SPSW, were considered based on the details used in the experimental specimens (Dubina and Dinu 2014). Load displacement type control and cyclic loading were applied to finite element models. Boundary and support conditions included rigid floor support and side supports to prevent the out-of-plane displacement frame. Fig. 4(b) shows boundary conditions and the place of cyclic loading. As shown in Fig. 4(b), all degrees of freedom at the base of piers' shear walls are closed. According to the general coordinates shown in Fig. 4(b), a cyclic load is applied to the x-direction to the reference point (*RP-1 and RP-2*). Also, according to the boundary conditions of the experimental setup (Dubina and Dinu 2014), to prevent the out-of-plane displacements, lateral supports in the panel zone were used (Fig. 4(b)). According to the experimental (Dubina and Dinu 2014) protocol of the specimens, the displacement type of loading was applied cyclically. In order to consider the initial imperfections of the web plates, a first of mode shapes was considered in the C-SPSW models. In addition, a buckling analysis was performed for the buckling to form a diagonal tensile field in the shear wall plate with the buckling mode shapes employed to create the initial imperfection (Deng *et al.* 2019, Mohebkhah and Azandariani 2020, Shariati *et al.* 2019). This was achieved by initially performing an eigen buckling analysis to determine the first buckling mode before the nonlinear analysis. The applied imperfection magnitude was considered $L/1000$, where L is the web plate width. These deformations were proportional to the eigen-mode shapes of the elastic buckling.

3.3 Material and properties

Material properties modeling uses steel material J_2 for beams, columns, and infill plate members (Chatterjee *et al.* 2015). For all models, the behavior of the materials was considered inelastic. The stress-strain curve was a bilinear model, and the plasticity model used was based on

Table 2 Material properties of the test (Dubina and Dinu 2014) specimens and used FE models

Element	Steel grade	Thickness (mm)	Material properties		
			Modulus of elasticity (GPa)	Yield stress (Mpa)	Ultimate stress (MPa)
HEB 240	S355	17	200	457	609
		10	200	458	609
HEB 180	S355	14	200	360	515
		8.5	200	408	540
HEA 180	S355	9.5	200	419	558
		6	200	415	542
Infill plate	S235	2	200	305	429

Von-Mises yield surface and associated flow rule. Plastic strain hardening was also considered using the nonlinear combination isotropic and kinematic hardening law (Gorji Azandariani *et al.* 2020a, c, 2021d, f). Combined isotropic and kinematic hardening model is available in ABAQUS software as a tool in the materials section, which is parameterized as (Hardening: Combined; Data type: Stabilized model). The input parameters in this model are in the feature of stress–strain data obtained from the experiment, also the ideal multi-line graph is following the stress–strain diagram of the test (Rahnavard *et al.* 2020). The properties of the test material of the steel coupons of the specimens tested by Dubina and Dinu (2014) and employed in the finite element modeling for infill plates, beams, and columns are reported in Table 2.

4. Validation of finite element model

In this part of the research, the accuracy of the finite element modeling of coupled steel plate shear walls was investigated using ABAQUS software. For this purpose, laboratory samples of the coupled steel plate shear walls of Dubina and Dinu (2014) and steel plate shear walls of Kharrazi (2005) were used for validation. During experiments, to investigate the behavior of thin steel plate shear walls, Dubina and Dinu (2014) tested two samples of two-story steel plate shear walls with a scale of 1:2 under uniform and cyclic loading. During experiments, to investigate the behavior of thin steel plate shear walls, Kharrazi (2005) tested two samples of two-story steel plate shear walls with a scale of 1:3 under cyclic loading. As these experimental specimens have been tested on two floors, they were selected for modeling and validation. The dimensions and details of the model connections are shown in Fig. 5. Two models were selected for modeling, the specifications of both test specimens being the same, while only the type of loading was different. The thickness of the infill plates was 2 mm, and the axis distance of the columns was 1400 mm. Table 3 presents the specifications of the Dubina and Dinu (2014) test specimens. The properties of the test material of the steel coupons of the specimens tested by Dubina and Dinu (2014) and employed in the finite element modeling for infill plates, beams, and columns are reported in Table 2.

4.1 Model R-M-T2

The analysis of the finite element model and the R-M-T2 test specimen are presented in Fig. 6. A comparison of the numerical model results and test specimen uniform loading shows that the model can simulate the behavior of the laboratory model. The maximum displacement applied in the R-M-T2 test (Dubina and Dinu 2014) specimen was 182 mm, and the maximum load was 1143 kN. The maximum force tolerated by the numerical model was 1155.7 kN, with the ratio of the results of the finite element model to the test being 1.01.

Table 3 Specifications of the test specimens of Dubina and Dinu (2014) and Kharrazi (2005)

Specimen	Plate thickness (mm)	Beam-to-column connection	Ext. column section	Int. column section	Beam section	Link beam section	Loading
R-M-T2	2	Rigid	HEB240	HEB180	HEA180	HEA180	Monotonic
R-C-T2	2	Rigid					Cyclic
DSPW-1	0.7	Rigid					Cyclic
DSPW-2	0.7	Rigid	2HSS102	-	W8×58	-	Cyclic

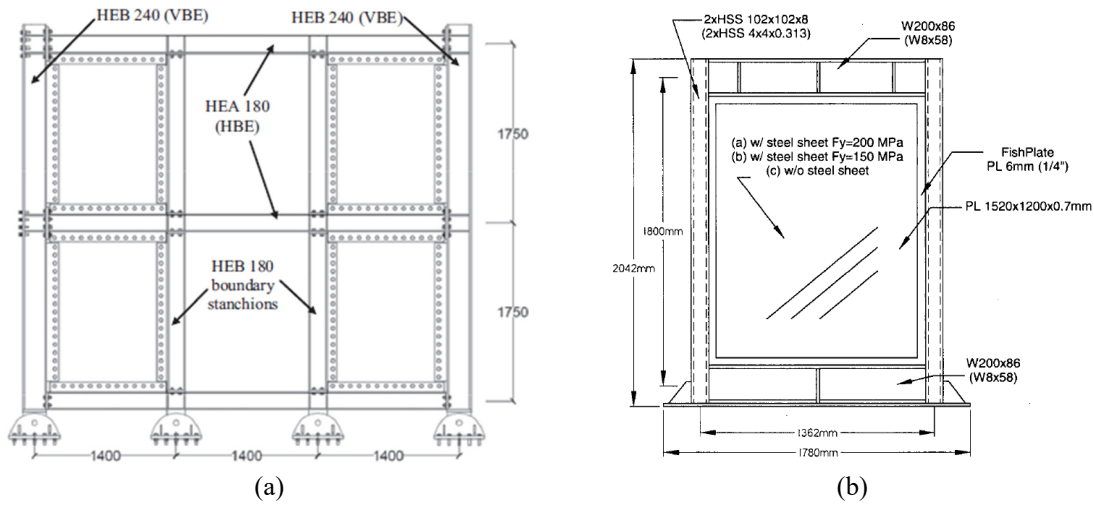


Fig. 5 Dimensions and geometry of the test specimens: (a) Dubina and Dinu (2014) and (b) Kharrazi (2005)

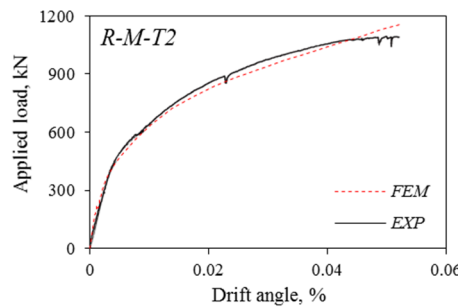


Fig. 6 Comparison of test (Dubina and Dinu 2014) results and finite element model R-M-T2

4.2 Model R-C-T2

The results of the analysis of the R-C-T2 finite element model under cyclic loading are shown in Fig. 7. A comparison of the results of the cyclic loading of the numerical model and the test specimen indicates that the model has been well able to simulate the hysteresis behavior of the laboratory model. The maximum displacement applied in the R-C-T2 test (Dubina and Dinu 2014) specimen was 182 mm, and the maximum load was 1151 kN. The maximum force tolerated by the numerical model was 1144 kN, with the ratio of the results of the finite element model to the test being 0.99. Comparison of the finite element analysis results and the test results reveal that the hysteresis behavior has predicted the initial stiffness of the loading and unloading, the permanent out-of-plane deformation, the stiffness, and the pinching phenomenon at the cyclic loading.

4.3 Model DSPW-1 and DSPW-2

The results of the analysis of the DSPW-1 and DSPW-2 finite element model under cyclic loading are shown in Fig. 8. A comparison of the results of the cyclic loading of the numerical

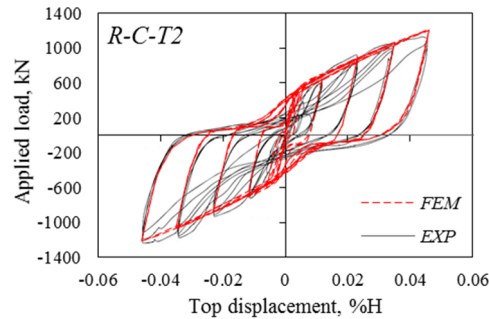


Fig. 7 Comparison of test (Dubina and Dinu 2014) results and finite element model R-C-T2

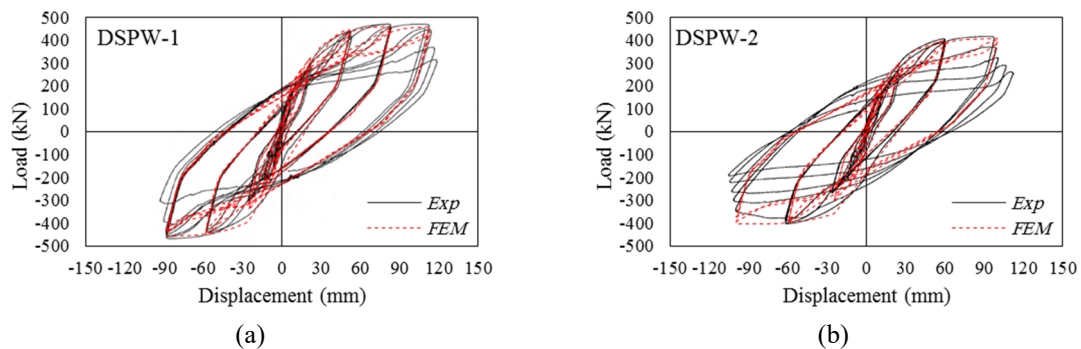


Fig. 8 Comparison of test (Kharrazi 2005) results and finite element model: (a) DSPW-1 and (b) DSPW-2

model and the test specimen indicates that the model has been well able to simulate the hysteresis behavior of the laboratory model. Comparison of the finite element analysis results and the test results reveal that the hysteresis behavior has predicted the initial stiffness of the loading and unloading, the permanent out-of-plane deformation, the stiffness, and the pinching phenomenon at the cyclic loading. Next, the nonlinear finite element method was used for validation to investigate the cyclic behavior of the coupled steel plate shear wall a fuse pin in the link beam (CF-SPSW).

5. Cyclic behavior of Coupled Steel Plate Shear Wall (C-SPSW)

5.1 The finite element models studied

To study the cyclic behavior of the C-SPSW with fuse pin in the link beam, it was selected to represent the last three floors of the 12-story structure designed at second 2. According to Fig. 3, the perimeter gravity frame bays, 5.0 m long, the SPSW bay, 5.0 m long, and the link beam bay, 2.5 m long, were considered from the center to center of the columns. The floors had the same height of 4 meters, and the frames were considered in two directions with five bays. The dimensions and sections used along with the plate thickness are presented in Table 4. Finite element models included coupled steel plate shear wall with I-shaped link beam, I-shaped link beam with reduced beam section (RBS), hollow-link beam with RBS, and fuse pin-link beam.

Table 4 Geometric and material properties of FE models

Model	Type of link beam	Geometric property of models	Yielding stress (MPa)			Length link beam (m)
			Plate	Beam & Link beam	Column	
C-S-I	I-section	Plate thickness: 3 mm Column: W24×131	310	410	410	2.5
C-S-RBS	RBS-section	Upper floors beam: W24×194	310	410	410	2.5
C-S-H	Hol. RBS- sections	Middle floors beam: W18×60 Link beams: W18×60	310	410	410	2.5
C-S-fuse	fuse	fuse: Circular pin D200 mm	310	310	410	1.5

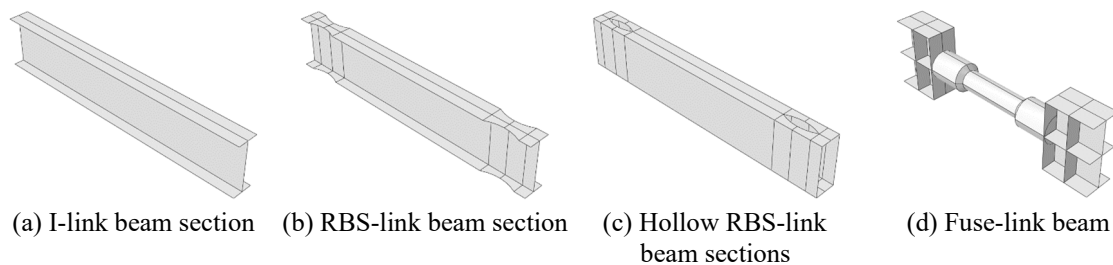


Fig. 9 Type of link beam in FE models

Fig. 9 displays the geometry of the link beams of the finite element models. For the I-shaped beam, a cross-section of W18×60 was used according to Fig. 9(a). The dimensions of the reduced cross-section were calculated according to FEMA-350 (2000), with values of $a = 100$ mm, $b = 320$ mm, $c = 40$ mm and $R = 340$ mm, respectively (Fig. 9(b)). A hollow rectangular beam was selected to obtain a weight of section W18×60. For this purpose, the hollow section flange thickness was equal to W18×60, and the web thickness of each side of the hollow section was equal to half the web thickness of W18×60. The reduced cross-section was also used for the hollow section, as displayed in Fig. 9(c). The fuse pin-link beam shown in Fig. 9(d) was selected according to reference (Dougka *et al.* 2014). For the yield zone to occur away from the pin-to-beam connection, the diameter of the pin-to-beam connection was greater than the middle region. The diameter of the pin in the middle region was 200 mm, and the diameter of the side regions was 300 mm. Also, the middle pin length was 700 mm, while the side pin length is 400 mm, as shown in Fig. 9(d). The material properties of the beams were columns of S355 steel with 410 MPa yield stress, while for infill plate and circular pin fuse of S235 steel with 310 MPa yield stress (Dubina and Dinu 2014), and Poisson coefficient 0.3 and modulus of elasticity 210 GPa were considered (Table 4). For the entire model, the behavior of the materials was inelastic, and the stress-strain curve was considered elastic-plastic perfect. The loading of the type displacement control and cyclic was applied at the top floor level. The ATC-24 (ATC-24 1992) protocol was used for cyclic loading in the finite element models (Fig. 10). The abbreviated names of finite element models are also presented in Table 4.

5.2 Results of finite element models

The finite element models of the coupled steel plate shear wall have been subjected to a quasi

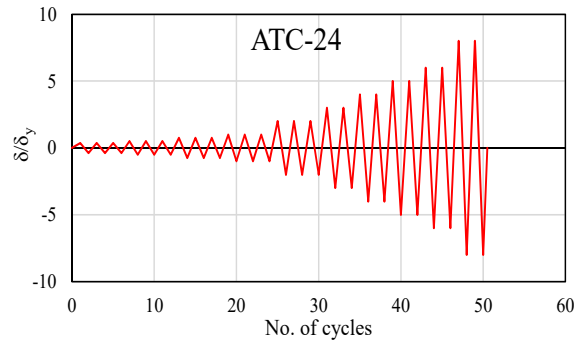


Fig. 10 Loading procedure applied in FE models

static analysis (explicit method) according to the ATC-24 (1992) protocol cyclic loading. The results of finite element models include hysteresis curves, lateral stiffness, and dissipation energy. The section presents the results of finite element models.

Finite element model C-S-I, a 3-span and 3-story C-SPSW, was used in the mid-span of the W60×18 cross-sections for link beams. The lateral load-displacement hysteresis curve of model C-S-I is shown in Fig. 11(a). Initial stiffness and maximum base shear strength were 113 kN/mm and 6682 kN, respectively. Fig. 12(a) displays the stress distribution in the contour of Von Mises model C-S-I. In Fig. 13(a), the Von Mises stress distribution of the link beams is revealed. Areas of maximum stress occurred in the proximity of the beam-column connections. C-S-RBS finite

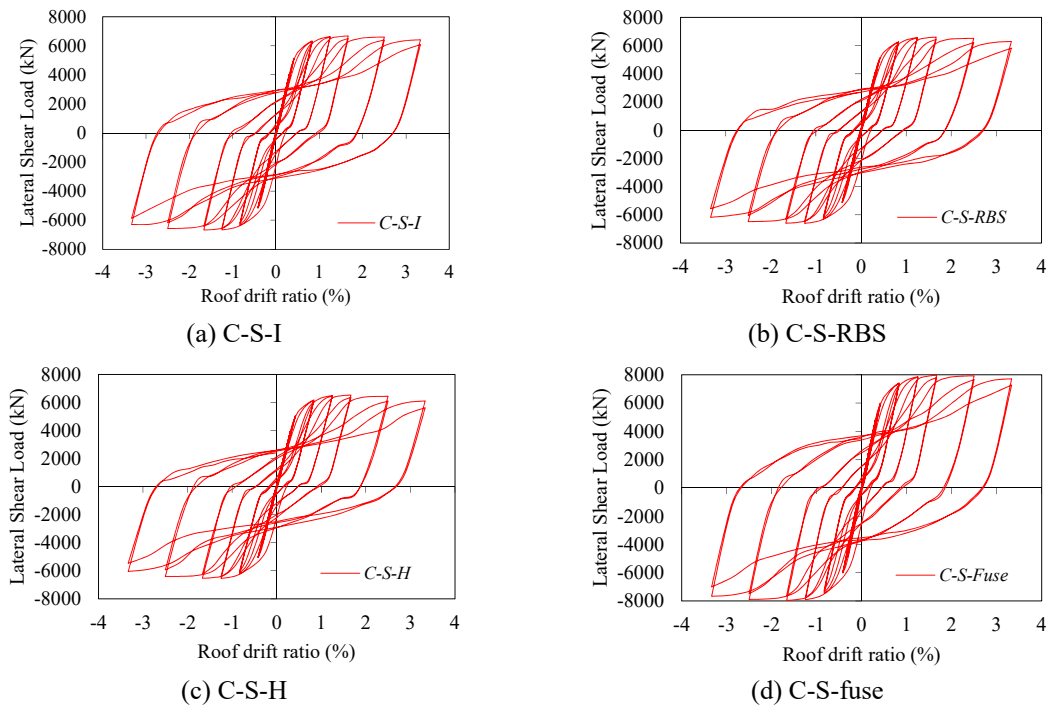


Fig. 11 Hysteretic lateral shear load – Roof drift ratio for models

element model, a 3-span and 3-story coupled steel plate shear wall, was used in the mid-span of W60×18 with a reduced cross-section (RBS) for link beams.

The lateral load-displacement hysteresis curve of model C-S-RBS is indicated in Fig. 10(b). Initial stiffness and maximum base shear strength were obtained at 112 kN/mm and 6602 kN. Fig. 11(b) demonstrates the stress distribution in the contour of Von Mises model C-S-RBS. Fig. 12(b) shows the Von Mises stress distribution of the reduced cross-section link beams. Due to the stress distribution, the maximum stress occurred at the reduced cross-section of the link beams. C-S-H finite element model, a 3-span and 3-story coupled steel plate shear wall, was used in the mid-span of the hollow section with an RBS for link beams.

The lateral load-displacement hysteresis curve of model C-S-H is shown in Fig. 11(c). Initial stiffness and maximum base shear strength were 110 kN/mm and 6534 kN, respectively. Fig. 12(c) indicates the stress distribution in the contour of Von Mises model C-S-H. Fig. 13(b) displays the Von Mises stress distribution of the hollow section link beams. Due to the stress distribution, the maximum stress occurred at the link beams' reduced cross-section and hollow web section. C-S-fuse finite element model, a 3-span and 3-story coupled steel plate shear wall, was used in the mid-span of fuse pin for link beams. The lateral load-displacement hysteresis curve of model C-S-fuse is shown in Fig. 11(d). Initial stiffness and maximum base shear strength were 135 kN/mm and 7966 kN, respectively. Fig. 12(d) demonstrates the stress distribution in the contour of Von Mises model C-S-fuse. Fig. 13(d) illustrates the Von Mises stress distribution of the fuse pin link beams. The Von Mises stress distribution results in Fig. 13(d) show that plastic hinges have been formed

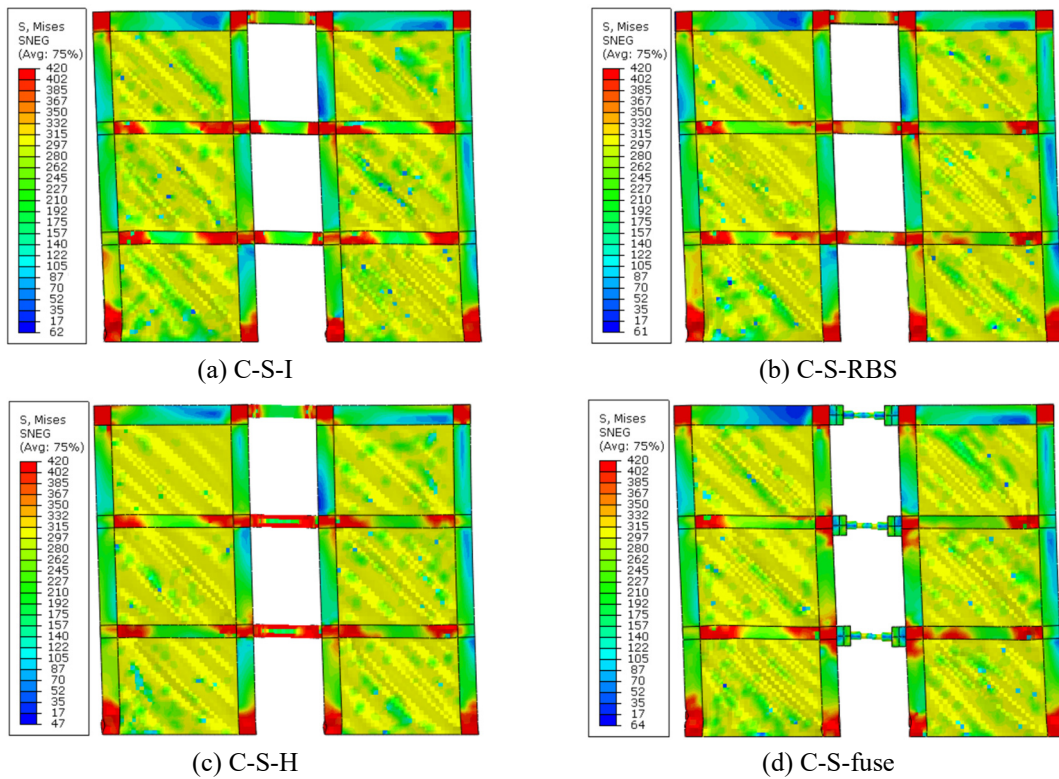


Fig. 12 Von Mises Stress distribution of FE model

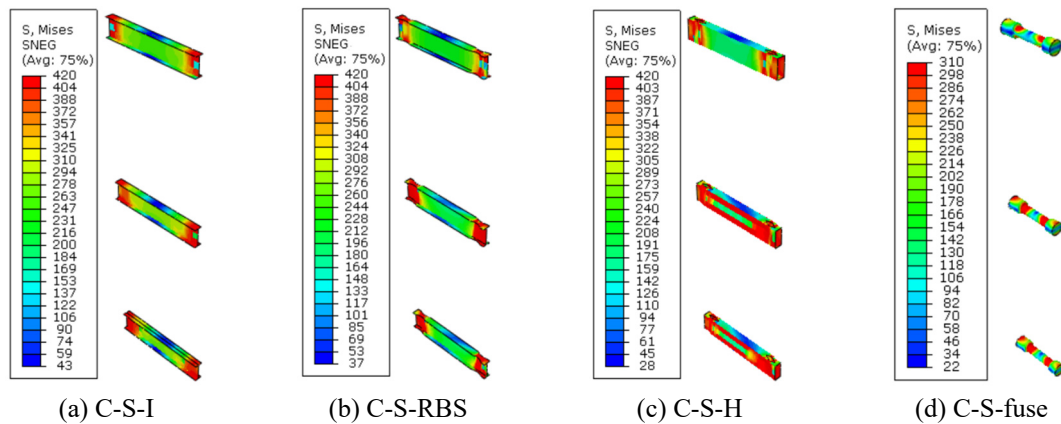


Fig. 13 Von Mises Stress distribution of link beams

in the fuse pins. According to Von Mises stress distribution, finite element models the column foot yields on the inner columns as well as the local buckling and yields of the external columns due to the internal axial force in the external columns. Also, the formation of plastic hinges occurred near the beam-to-columns connections. Further, with the formation of a tensile field in the infill plates, the shear yield of the plates in the finite element models is observed.

5.3 Comparison of finite element models

The envelope curves of all hysteresis curves are displayed in Fig. 14(a) to compare the general behavior of finite element models. Given the use of the fuses pin instead of typical link beams, the stiffness and ultimate capacity of the coupled steel plate shear walls have increased. The C-S-fuse model upper bound and the C-S-H model lower bound made this curve consider the ultimate capacity. To investigate the ultimate capacity and impact of the fuse pin in the finite element models of the coupled steel plate shear wall, the bar graph of Fig. 14(b) reveals the maximum base shear and the maximum normalized base shear relative to the C-S-I model. Given the maximum normalized base shear values, the impact of I-shaped beams with reduced cross-section, the hollow section with reduced cross-section, and fuse pin were 0.99, 0.98, and 1.19, respectively. The

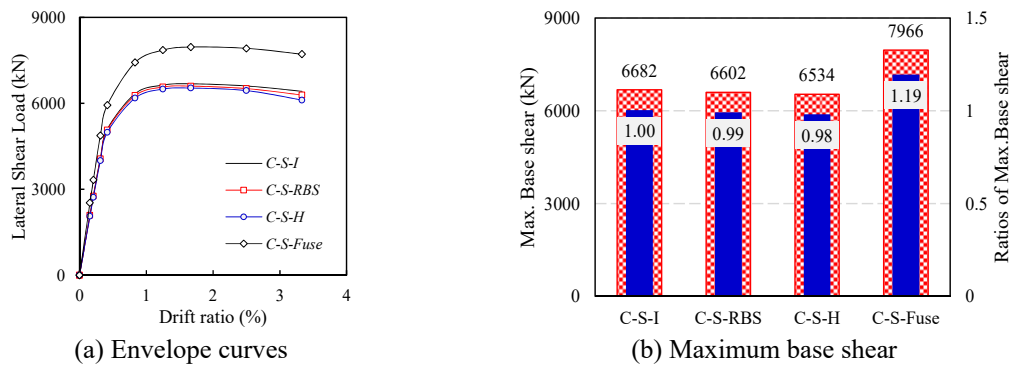


Fig. 14 Base shear of FE models

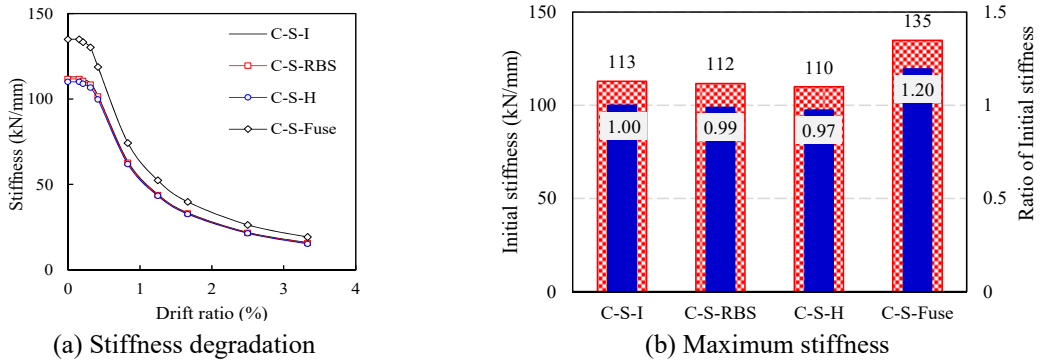


Fig. 15 Stiffness of FE models

results suggest that the coupled steel plate shear wall with the fuse pin-link beam has had a 19% increase in base shear compared to the typical coupled steel plate shear wall.

Fig. 15(a) indicates the variations in the stiffness secant of the finite element models to the drift ratio of the roof. The stiffness secant of each cycle plotted the slope of the line between the origin and the peak point of the cycle. According to Fig. 15(a), the rate of stiffness reduction is almost the same in all models. In all finite element models, up to 0.5% drift ratio, no dramatic variation has occurred in stiffness. Fig. 15(b) demonstrates the bar graph of the initial stiffness and the normalized stiffness. Compared to other models, the shear behavior of the fuse pin-link beam compared to other models has increased the initial stiffness of the coupled steel plate shear wall.

The surface enclosed within hysteresis loops has been used to compare the amount of energy dissipated by finite element models under cyclic loading. In this study, the finite element models were calculated from the intra-loop surface hysteresis, with the cumulative dissipation energy values to the drift ratio being shown in Fig. 16(a). According to the hysteresis shapes and loops of Fig. 11, it is observed that the C-S-fuse model has had more energy dissipation than the other finite element models. The cause of this behavior in the C-S-fuse model is due to the shear behavior of the fuse pin element and the flexural behavior of the other link beams. According to Fig. 16(a), three C-SPSW models with C-S-I, C-S-RBS, and C-S-H reveal a similar energy-absorbing behavior. Fig. 16(b) displays the bar graph of the total energy dissipation and the total normalized

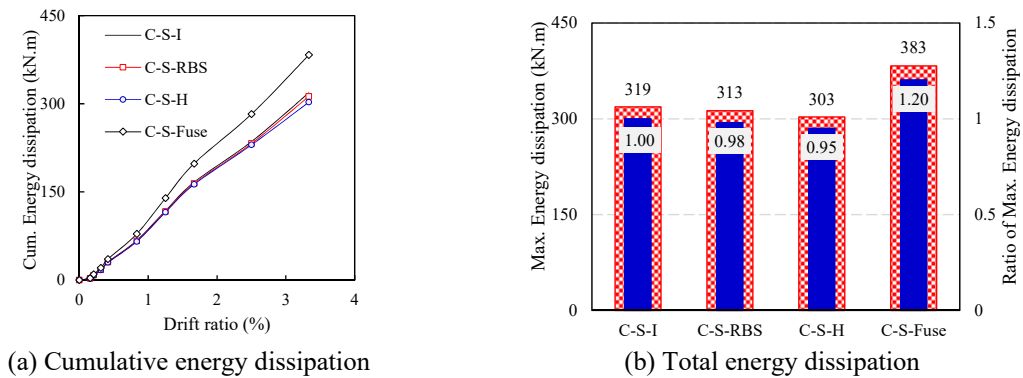


Fig. 16 Energy dissipation of FE models

energy. The results indicate that the coupled steel plate shear wall with the fuse pin-link beam has a 20% increase in total energy dissipation compared to the typical coupled steel plate shear wall.

6. Nonlinear time-history analysis

This section investigates the nonlinear time-history analysis of the coupled steel plate shear wall with fuse pin, which is designed in Sec. 2, was paid under seismic loading. The process of evaluating the nonlinear time-history analysis requires a set of earthquake records that can be used to analyze the designed structures dynamically C-SPSW. A set of remote domain records is considered in this study, which includes 12 records selected from the PEER NGA database based on FEMA P-695 (2009). All specifications of the selected ground motions for far-field earthquakes are shown in Table 5. Fig. 17 shows the response spectrum of the ground motions along with the mean of the records and the design response spectrum. Also, $S_a(T1,5\%)$ has been selected as the spectral acceleration at the time of period of the first mode, along with 5% damping to display the intensity index.

The drift ratio of each floor is calculated for C-SPSW structures 12-story for all ground motions and is shown in Fig. 18(a). Also, the average floor drift ratio is calculated for 12 ground motions and is exhibited in Fig. 18(a). As shown in Fig. 18(a), in a 12-story of C-SPSW structure, the maximum value of the drift ratio is 2.37 %, which occurred on the second floor. The drift ratio of each floor is calculated for C-SPSW with fuse pin structures 12-story for all ground motions and is shown in Fig. 18(b). Also, the average floor drift ratio is calculated for 12 ground motions and is exhibited in Fig. 18(b). As shown in Fig. 18(a), in a 12-story of C-SPSW with fuse pin structure, the maximum value of the drift ratio is 1.32 %, which occurred on the second floor. To compare the drift ratio of the floors, the diagram of the average drift ratio of the floors to the height of the structure is presented in Fig. 18(c) for the structures of coupled steel plate shear wall and coupled steel shear wall with yielding fuse pin. Comparison of the results shows that, in general, the use of surrendered fuses in the connection beam has reduced the drift ratio to the structure. This reduction

Table 5 Seismic parameters of the selected ground motions

GM	Name earthquake	Year	Magnitude	Site-to source epicentral distance (km)	PGA_{max} (g)	PGV_{max} (cm/s.)
GM01	Hector Mine	1999	7.1	11.7	0.34	42
GM02	Imperial Valley	1979	6.5	22	0.35	33
GM03	Kocaeli, Turkey	1999	7.5	15.4	0.36	59
GM04	Landers	1992	7.3	23.6	0.24	52
GM05	Superstition Hills	1987	6.5	18.2	0.36	46
GM06	Cape Mendocino	1992	7.0	14.3	0.55	44
GM07	Chi-Chi, Taiwan	1999	7.6	10	0.44	115
GM08	Loma Prieta	1989	6.9	15.2	0.53	35
GM09	Manjil, Iran	1990	7.4	12.6	0.51	54
GM10	Duzce, Turkey	1999	7.1	12	0.82	62
GM11	Northridge	1994	6.7	17.2	0.52	63
GM12	Kobe, Japan	1995	6.9	7.1	0.51	37

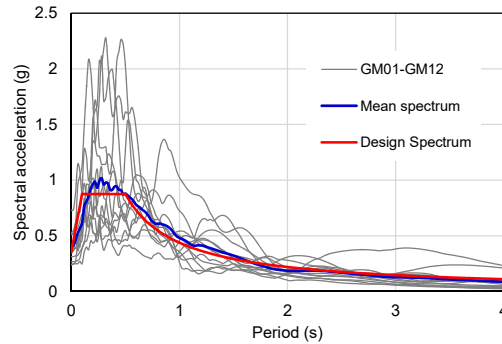


Fig. 17 Mean spectrum of the far-field ground motions scaled based on Sa(T1) and design spectrum

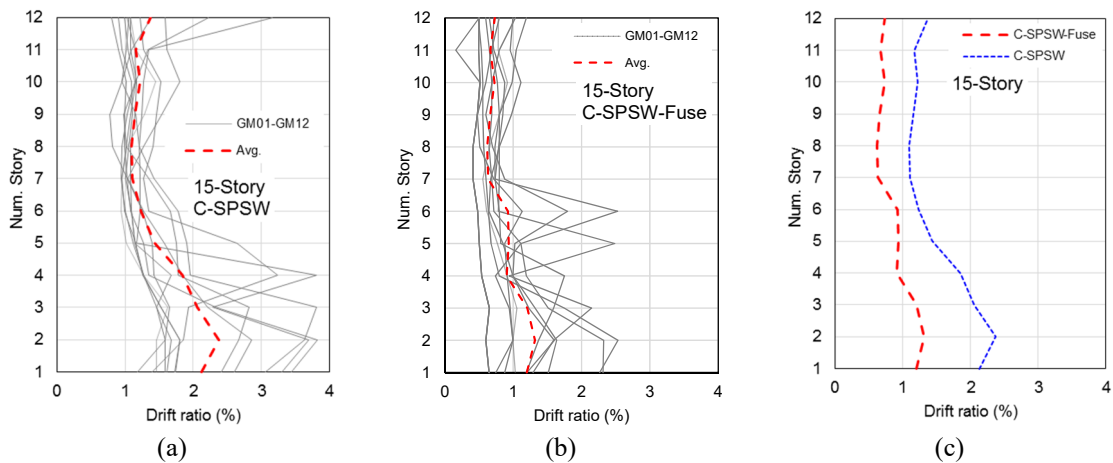


Fig. 18 Drift ratio of structures: (a) C-SPSW; (b) C-SPSW with fuse pin; and (c) Comparison C-SPSW; and C-SPSW with fuse pin

in drift ratio is mostly limited to the lower floors, and also, the average reduction of thrust in the 12-story structure is 52.9% on average at the height of the structure. According to the results of floor drift, the use of surrendered fuse as a ductile element has reduced the drift ratio in the structure's height.

7. Future works and current study limitations

In the future, there are still many numerical and experimental works that need to be considered to develop and expand the analysis and design of coupled-steel plate shear wall with fuse pin systems. Currently, due to the limitations of performing experimental work with a large number of specimens, challenges have been identified in evaluating the performance of steel shear wall systems. Such experimental work needs to take more time, leading to increased costs. However, the coupled-steel plate shear wall with fuse pin systems is still a novelty. Extensive further research is still needed to establish a comprehensive body of information about of the coupled-

steel plate shear wall with fuse pin. However, there are still clear gaps in the seismic analysis and design of the coupled-steel plate shear wall with fuse pin systems. Hence, studies on this aspect are still scarce and provide an opportunity to explore further research in this area. Further research and future work can be done to investigate the seismic behavior and performance of coupled-steel plate shear wall with fuse pin systems with the aim of improving seismic performance and reducing the cost of upgrading and amplifying the fuse element. In this context, can mention the development of approaches such as design based on performance and capacity methods for the coupled-steel plate shear wall with fuse pin system. It is hoped that the present study will contribute to the development of appropriate design approaches and insight to achieving performance goals and improving the performance of the coupled-steel plate shear wall with fuse pin systems systems.

8. Conclusions

In this research, an innovative system of coupled steel plate shear wall with fuse pin was presented. Finite element method and cyclic analysis were performed to investigate the behavior of the innovative coupled steel plate shear wall with a fuse pin-link beam. Two test specimens of a two-story coupled steel plate shear wall were modeled to verify the finite element method results. The analysis of finite element models shows that it has a good prediction of hysteresis behavior of coupled steel plate shear wall. The finite element models include coupled steel plate shear wall with I-shaped link beam, I-shaped link beam with reduced beam section (RBS), and hollow-link beam with RBS and fuse pin-link beam. According to the results, the reduced sections used in link beams did not affect the stiffness, energy dissipation, and ultimate capacity. The results revealed that the fuse pin-link beam increased the base shear by 19% compared to other link beams. Due to the shear behavior of the fuse pin-link beam compared to other models, it has enhanced the initial stiffness of the coupled steel plate shear wall. According to the hysteresis loops, the coupled steel plate shear wall with the fuse pin-link beam had more energy dissipation than other finite element models. The rate of total energy dissipation in the model with the fuse pin in the link beam was approximately 20% more than the other models. The cause of this behavior in the C-S-fuse model over other finite element models is due to the shear behavior of the pin element and the flexural behavior of other link beams.

References

- ABAQUS-6.10 (2010), Standard user's manual. Hibbitt, Karlsson and Sorensen, Inc.
- AISC (2007), Steel design guide 20, steel plate shear walls, Chicago, IL, USA.
- AISC 341-16 (2016), AISC Seismic Provisions for Structural Steel Buildings, (ANSI/AISC 341-16), USA.
- Ali, M.M., Osman, S.A., Husam, O.A. and Al-Zand, A.W. (2018), "Numerical study of the cyclic behavior of steel plate shear wall systems (SPSWs) with differently shaped openings", *Steel Compos. Struct., Int. J.*, **26**(3), 361-373. <https://doi.org/10.12989/scs.2018.26.3.361>
- ASCE7-10 (2010), Minimum Design Loads for Buildings and Other Structures, Standards, American Society of Civil Engineers, Reston, VA, USA.
- ATC-24 (1992), California, USA.
- Borello, D.J. and Fahnestock, L.A. (2012), "Behavior and mechanisms of steel plate shear walls with coupling", *J. Constr. Steel Res.*, **74**, 8-16. <https://doi.org/10.1016/j.jcsr.2011.12.009>
- Borello, D.J. and Fahnestock, L.A. (2013), "Seismic design and analysis of steel plate shear walls with coupling", *J. Struct. Eng.*, **139**(8), 1263-1273. [https://doi.org/10.1061/\(ASCE\)ST.1943-541X.0000576](https://doi.org/10.1061/(ASCE)ST.1943-541X.0000576)

- CAN/CSA-S16-09 (2009), Rexdale, Ontario, Canada, Canadian Standards Association.
- Chatterjee, A.K., Bhowmick, A. and Bagchi, A. (2015), "Development of a simplified equivalent braced frame model for Steel Plate Shear Wall systems", *Steel Compos. Struct., Int. J.*, **18**(3), 711-737.
<https://doi.org/10.12989/scs.2015.18.3.711>
- Deng, E.F., Zong, L. and Ding, Y. (2019), "Numerical and analytical study on initial stiffness of corrugated steel plate shear walls in modular construction", *Steel Compos. Struct., Int. J.*, **32**(3), 347-359.
<https://doi.org/10.12989/scs.2019.32.3.347>
- Dhar, M.M. and Bhowmick, A.K. (2016), "Seismic response estimation of steel plate shear walls using nonlinear static methods", *Steel Compos. Struct., Int. J.*, **20**(4), 777-799.
<https://doi.org/10.12989/scs.2016.20.4.777>
- Dimakogianni, D., Dougka, G., and Vayas, I. (2015), "Seismic behavior of frames with innovative energy dissipation systems (FUSEIS1-2)", *Eng. Struct.*, **90**, 83-95. <https://doi.org/10.1016/j.engstruct.2015.01.054>
- Dougka, G., Dimakogianni, D. and Vayas, I. (2014), "Innovative energy dissipation systems (FUSEIS 1-1) - Experimental analysis", *J. Constr. Steel Res.*, **96**, 69-80. <https://doi.org/10.1016/j.jcsr.2014.01.003>
- Dubina, D., and Dinu, F. (2014), "Experimental evaluation of dual frame structures with thin-walled steel panels", *Thin-Wall. Struct.*, **78**, 57-69. <https://doi.org/10.1016/j.tws.2014.01.001>
- Elgaaly, M., Caccese, V. and Du, C. (1993), "Postbuckling behavior of steel-plate shear walls under cyclic loads", *J. Struct. Eng.*, **119**(2), 588-605. [https://doi.org/10.1061/\(ASCE\)0733-9445\(1993\)119:2\(588\)](https://doi.org/10.1061/(ASCE)0733-9445(1993)119:2(588))
- FEMA 350 (2000), Federal Emergency Management Agency, Recommended Seismic Design Criteria for New Steel Moment-Frame Buildings, Washington, DC, USA.
- FEMA P695 (2009), Quantification of building seismic performance factors, Technical Report P695, Applied Technology Council for the Federal Emergency Management Agency, Washington, DC, USA.
- Formisano, A., Mazzolani, F.M. and De Matteis, G. (2007), "Numerical analysis of slender steel shear panels for assessing design formulas", *Int. J. Struct. Stab. Dyn.*, **7**(02), 273-294.
<https://doi.org/10.1142/S0219455407002289>
- Gorji Azandariani, M., Abdolmaleki, H. and Gorji Azandariani, A. (2020a), "Numerical and analytical investigation of cyclic behavior of steel ring dampers (SRDs)", *Thin-Wall. Struct.*, **151**, 106751.
<https://doi.org/10.1016/j.tws.2020.106751>
- Gorji Azandariani, M., Gholhaki, M. and Kafi, M.A. (2020b), "Experimental and numerical investigation of low-yield-strength (LYS) steel plate shear walls under cyclic loading", *Eng. Struct.*, **203**, 109866.
<https://doi.org/10.1016/j.engstruct.2019.109866>
- Gorji Azandariani, M., Gholhaki, M. and Kafi, M.A. (2021a), "Hysteresis finite element model for evaluation of cyclic behavior and performance of steel plate shear walls (SPSWs)", *Structures*, **29**, 30-47.
<https://doi.org/https://doi.org/10.1016/j.istruc.2020.11.009>
- Gorji Azandariani, M., Gholhaki, M., Kafi, M.A. and Zirakian, T. (2021b), "Study of effects of beam-column connection and column rigidity on the performance of SPSW system", *J. Build. Eng.*, **33**.
<https://doi.org/10.1016/j.jobe.2020.101821>
- Gorji Azandariani, M., Gholhaki, M., Kafi, M.A., Zirakian, T., Khan, A., Abdolmaleki, H. and Shojaeifar, H. (2021c), "Investigation of performance of steel plate shear walls with partial plate-column connection (SPSW-PC)", *Steel Compos. Struct., Int. J.*, **39**(1), 109-123. <https://doi.org/10.12989/scs.2021.39.1.109>
- Gorji Azandariani, M., Gorji Azandariani, A. and Abdolmaleki, H. (2020c), "Cyclic behavior of an energy dissipation system with steel dual-ring dampers (SDRDs)", *J. Constr. Steel Res.*, **172**, 106145.
<https://doi.org/10.1016/j.jcsr.2020.106145>
- Gorji Azandariani, M., Kafi, M.A. and Gholhaki, M. (2021d), "Innovative hybrid linked-column steel plate shear wall (HLCS) system: Numerical and analytical approaches", *J. Build. Eng.*, **43**, 102844.
<https://doi.org/10.1016/j.jobe.2021.102844>
- Gorji Azandariani, M., Rousta, A.M., Mohammadi, M., Rashidi, M. and Abdolmaleki, H. (2021e), "Numerical and analytical study of ultimate capacity of steel plate shear walls with partial plate-column connection (SPSW-PC)", *Structures*, **33**, 3066-3080. <https://doi.org/10.1016/j.istruc.2021.06.046>
- Gorji Azandariani, M., Rousta, A.M., Usefvand, E., Abdolmaleki, H. and Gorji Azandariani, A. (2021f), "Improved seismic behavior and performance of energy-absorbing systems constructed with steel rings",

- Structures*, **29**, 534-548. <https://doi.org/10.1016/j.istruc.2020.11.041>
- Hassanipour, A., Rahnavard, R., Mokhtari, A. and Rahnavard, N. (2015), "Numerical investigation on reduced beam web section moment connections under the effect of cyclic loading", *J. Multidiscip. Eng. Sci. Technol. (JMEST)*, **2**(8), 2054-2061.
- Hjelmstad, K.D. and Popov, E.P. (1983), "Cyclic behavior and design of link beams", *J. Struct. Eng.*, **109**(10), 2387-2403. [https://doi.org/10.1061/\(ASCE\)0733-9445\(1983\)109:10\(2387\)](https://doi.org/10.1061/(ASCE)0733-9445(1983)109:10(2387))
- IS2800 (2014), Iranian Code of Practice for Seismic Resistant Design of Buildings, Standard No. 2800, Tehran, Iran.
- Ji, X., Wang, Y., Ma, Q. and Okazaki, T. (2016), "Cyclic behavior of very short steel shear links", *J. Struct. Eng.*, **142**(2). [https://doi.org/10.1061/\(ASCE\)ST.1943-541X.0001375](https://doi.org/10.1061/(ASCE)ST.1943-541X.0001375)
- Ji, X., Wang, Y., Ma, Q. and Okazaki, T. (2017), "Cyclic behavior of replaceable steel coupling beams", *J. Struct. Eng.*, **143**(2). [https://doi.org/10.1061/\(ASCE\)ST.1943-541X.0001661](https://doi.org/10.1061/(ASCE)ST.1943-541X.0001661)
- Kharrazi, M.H. (2005), "Rational method for analysis and design of steel plate shear walls", Ph.D. Dissertation; University of British Columbia, Vancouver, Canada.
- Li, C.H., Tsai, K.C., Chang, J.T. and Lin, C.H. (2011), "Cyclic test of a coupled steel plate shear wall substructure", *Procedia Eng.*, 582-589. <https://doi.org/10.1016/j.proeng.2011.07.073>
- Li, C.-H., Tsai, K.-C., Chang, J.-T., Lin, C.-H., Chen, J.-C., Lin, T.-H. and Chen, P.-C. (2012), "Cyclic test of a coupled steel plate shear wall substructure", *Earthq. Eng. Struct. Dyn.*, **41**(9), 1277-1299. <https://doi.org/10.1002/eqe.1180>
- Lubell, A.S., Prion, H.G.L., Ventura, C.E. and Rezai, M. (2000), "Unstiffened steel plate shear wall performance under cyclic loading", *J. Struct. Eng.*, **126**(4), 453-460. [https://doi.org/10.1061/\(ASCE\)0733-9445\(2000\)126:4\(453\)](https://doi.org/10.1061/(ASCE)0733-9445(2000)126:4(453))
- Malley, J.O. and Popov, E.P. (1984), "Shear links in eccentrically braced frames", *J. Struct. Eng.*, **110**(9), 2275-2295. [https://doi.org/10.1061/\(ASCE\)0733-9445\(1984\)110:9\(2275\)](https://doi.org/10.1061/(ASCE)0733-9445(1984)110:9(2275))
- Mohebbkhah, A. and Azandariani, M.G. (2020), "Shear resistance of retrofitted castellated link beams: Numerical and limit analysis approaches", *Eng. Struct.*, **203**, 109864. <https://doi.org/10.1016/j.engstruct.2019.109864>
- Okazaki, T., Arce, G., Ryu, H.C. and Engelhardt, M.D. (2005), "Experimental study of local buckling, overstrength, and fracture of links in eccentrically braced frames", *J. Struct. Eng.*, **131**(10), 1526-1535. [https://doi.org/10.1061/\(ASCE\)0733-9445\(2005\)131:10\(1526\)](https://doi.org/10.1061/(ASCE)0733-9445(2005)131:10(1526))
- Park, H.-G., Kwack, J.-H., Jeon, S.-W., Kim, W.-K. and Choi, I.-R. (2007), "Framed Steel Plate Wall Behavior under Cyclic Lateral Loading", *J. Struct. Eng.*, **133**(3), 378-388. [https://doi.org/10.1061/\(ASCE\)0733-9445\(2007\)133:3\(378\)](https://doi.org/10.1061/(ASCE)0733-9445(2007)133:3(378))
- Popov, E.P. and Engelhardt, M.D. (1988), "Seismic eccentrically braced frames", *J. Constr. Steel Res.*, **10**(C), 321-354. [https://doi.org/10.1016/0143-974X\(88\)90034-X](https://doi.org/10.1016/0143-974X(88)90034-X)
- Qin, Y., Lu, J.Y., Huang, L.C.X. and Cao, S. (2017), "Flexural behavior of beams in steel plate shear walls", *Steel Compos. Struct., Int. J.*, **23**(4), 473-481. <https://doi.org/10.12989/scs.2017.23.4.473>
- Rahnavard, R., Hassanipour, A. and Siahpolo, N. (2015), "Analytical study on new types of reduced beam section moment connections affecting cyclic behavior", *Case Stud. Struct. Eng.*, **3**, 33-51. <https://doi.org/10.1016/j.csse.2015.03.001>
- Rahnavard, R., Hassanipour, A. and Mounesi, A. (2016), "Numerical study on important parameters of composite steel-concrete shear walls", *J. Constr. Steel Res.*, **121**, 441-456. <https://doi.org/10.1016/j.jcsr.2016.03.017>
- Rahnavard, R., Hassanipour, A., Suleiman, M. and Mokhtari, A. (2017), "Evaluation on eccentrically braced frame with single and double shear panels", *J. Build. Eng.*, **10**, 13-25. <https://doi.org/10.1016/j.jobe.2017.01.006>
- Rahnavard, R., Rebelo, C., Craveiro, H.D. and Napolitano, R. (2020), "Understanding the cyclic performance of composite steel-concrete connections on steel bridges", *Eng. Struct.*, **224**, 111213. <https://doi.org/10.1016/j.engstruct.2020.111213>
- Shariati, M., Faegh, S.S., Mehrabi, P., Bahavarnia, S., Zandi, Y., Masoom, D.R., Toghroli, A., Trung, N.T., and Salih, M.N.A. (2019), "Numerical study on the structural performance of corrugated low yield point

- steel plate shear walls with circular openings”, *Steel Compos. Struct., Int. J.*, **33**(4), 569-581.
<https://doi.org/10.12989/scs.2019.33.4.569>
- Shekastehband, B., Azaraxsh, A.A. and Showkati, H. (2017), “Hysteretic behavior of perforated steel plate shear walls with beam-only connected infill plates”, *Steel Compos. Struct., Int. J.*, **25**(4), 505-521.
<https://doi.org/10.12989/scs.2017.25.4.505>
- Talebizadehsardari, P., Eyvazian, A., Gorji Azandariani, M., Nhan Tran, T., Kumar Rajak, D. and Babaei Mahani, R. (2020), “Buckling analysis of smart beams based on higher order shear deformation theory and numerical method”, *Steel Compos. Struct., Int. J.*, **35**(5), 635-640.
<https://doi.org/https://doi.org/10.12989/scs.2020.35.5.635>
- Vatansever, C. and Berman, J.W. (2015), “Analytical investigation of thin steel plate shear walls with screwed infill plate”, *Steel Compos. Struct., Int. J.*, **19**(5), 1145-1165.
<https://doi.org/10.12989/scs.2015.19.5.1145>
- Vatansever, C. and Yardimci, N. (2011), “Experimental investigation of thin steel plate shear walls with different infill-to-boundary frame connections”, *Steel Compos. Struct., Int. J.*, **11**(3), 251-271.
<https://doi.org/10.12989/scs.2011.11.3.251>
- Wang, M., Shi, Y., Xu, J., Yang, W. and Li, Y. (2015), “Experimental and numerical study of unstiffened steel plate shear wall structures”, *J. Constr. Steel Res.*, **112**, 373-386.
<https://doi.org/10.1016/j.jcsr.2015.05.002>